Effect of the Metal on Electron Transfer across Self-Assembled Monolayers

H. O. Finklea,* K. Yoon, E. Chamberlain, J. Allen, and R. Haddox

Department of Chemistry, West Virginia University, Morgantown, West Virginia 26506-6045

Received: November 9, 2000; In Final Form: February 1, 2001

Electron-transfer kinetic measurements are made on one type of self-assembled monolayer {$HS(CH_2)_{15}COOH$ with attached [$Ru^{II}(NH_3)_5$(4-aminomethylpyridine)]} on gold, platinum, and silver polycrystalline electrodes in one electrolyte at room temperature. Cyclic voltammograms over a wide range of scan rates are analyzed to extract the rate constants as a function of overpotential. Tafel plots are fitted to theoretical curves based on the Marcus DOS theory to obtain the standard rate constants and the reorganization energies. A reorganization energy of 0.8 ± 0.1 eV is obtained on all three metals. The standard rate constants for Au, Pt, and Ag are 1.0 ± 0.3, 1.7 ± 0.4, and 0.6 ± 0.2 s^{-1}. The results confirm the theoretical prediction that the electronic coupling of "d" band states in the metal to remote redox centers is weak.

Introduction

Marcus density-of-states (DOS) theory has been successfully applied to electron transfer between metal electrodes and redox molecules attached via self-assembled monolayers (SAMs).[1] The theory is based on an integrated overlap of donor and acceptor states modified with an electronic coupling term. Because of the separation of the metal and redox centers by the SAM, the electronic coupling is weak, and a nonadiabatic formalism is invoked. For a reduction (electron transfer from the metal to the attached redox center), the cathodic rate constant is given by the following equations:

$$k_{cat} = (2\pi/\hbar)\int D_{OX}(\epsilon,\lambda,\eta)\, f(\epsilon)|V|^2\, d\epsilon \quad (1)$$

$$D_{OX}(\epsilon,\lambda,\eta) = (4\pi\lambda k_B T)^{-1/2} \exp(-(\epsilon - \lambda - e\eta)^2/(4\lambda k_B T)) \quad (2)$$

$$f(\epsilon) = (1 + \exp(\epsilon/k_B T))^{-1} \quad (3)$$

$$|V|^2 = \rho(\epsilon)|H_{kA}|^2 \quad (4)$$

where ϵ is the energy of electron transfer (referenced to the Fermi energy of the metal), η is the overpotential ($\eta = E - E^{0\prime}$), λ is the reorganization energy, D_{OX} is the Gaussian distribution of acceptor states for the oxidized redox centers, f is the Fermi−Dirac distribution of occupied states in the metal, $|V|^2$ is the electronic coupling between metal donor and redox acceptor states, $\rho(\epsilon)$ is the density of metal states near the Fermi energy, and $|H_{kA}|^2$ is the electronic coupling between the redox acceptor state and an electronic state of wave vector k, averaged over all wave vectors.[2−4] Normally, the electronic coupling term and density of states are assumed to be independent of energy and are brought outside the integral. Several testable predictions arise from this theory, such as curved Tafel plots ($\ln(k)$ vs η) and the exponential decay of the rate constant with distance or number of repeating units in the SAM. An experimental Tafel plot can be fitted to the theoretical Tafel plots to obtain λ. The reorganization energy can also be obtained from measurement of the standard rate constant as a function of temperature via modified Arrhenius plots of $\ln(k/T^{1/2})$ vs $1/T$.[5]

These predictions are in good agreement with experiments on electrodes coated with alkanethiol SAMs.[1] Attached redox centers such as $pyRu(NH_3)_5^{2+}$,[6,7] ferrocene,[5,8−10] cytochrome *c*,[11−13] and a number of freely diffusing redox centers[14−16] display an exponential decay of the standard rate constant with the length of the alkyl chain. The tunneling parameter (slope of the $\ln(k)$ vs number of methylenes in the alkane chain) is -1.0 per CH_2, in agreement with a recent theoretical prediction.[3] Tafel plots exhibit the anticipated curvature and saturation of the rate constant at large overpotentials. Reorganization energies obtained from Tafel plots and modified Arrhenius plots are close to the values predicted by a simple Born model and are independent of the oxidation state.

Recently, Gosavi and Marcus examined the role of the metal on nonadiabatic electron-transfer kinetics.[2] The density of states near the Fermi energy $\rho(\epsilon)$ is a factor of 7.5 higher for Pt than it is for Au, due to the overlap of d band states with the Fermi energy in the former metal. However, the electronic coupling per state is considerably weaker for the d band states compared to the sp band states. The rationale is that d band states are more strongly localized and consequently are coupled less effectively to remote redox centers. Support for this idea appears in field emission experiments.[17] The net result is a predicted ratio of 1.8 for the rate constants on Pt relative to the rate constants on Au.

There have been previous reports of attempts to measure the rate of one redox reaction on several metals.[18−20] For example, Iwasita et al. measured the kinetics of $Ru(NH_3)_6^{3+/2+}$ at Pt, Au, Pd, Cu, Ag, and Hg electrodes in 1 M KF and found the standard rate constant to be nearly independent of the metal.[21] At bare metal electrodes, such measurements are compromised by double-layer effects and ambiguity about the electronic coupling between the metal and the ruthenium complex (adiabatic or nonadiabatic). Variations in the reorganization energy with the metal, which can affect the standard rate constant, are also unknown. Long-chain SAMs with attached redox centers offer a way of minimizing double-layer effects and simultaneously measuring λ. We report here the kinetics of one type of electroactive SAM on Au, Pt, and Ag.

10.1021/jp0041510 CCC: $20.00
Published on Web 03/21/2001

Experimental Section

$HS(CH_2)_{15}COOH$ and $[Ru^{II}(NH_3)_5(4\text{-aminomethylpyridine})](PF_6)_3$ [Ru(AMP)] were prepared as previous described.[6,22] Because the Ru complex is photosensitive, solutions and SAMs containing the complex were handled under reduced light conditions. 1,3-Dimethylaminopropyl-3-ethylcarbodiimide hydrochloride (EDC) was purchased from Aldrich.

All metal electrodes (Au, Pt, Ag) were formed by melting beads of 0.1−0.2 cm diameter on the end of the pure wire. Immersion of the bead and a minimal amount of wire in the electrolyte yielded an electrode area on the order of 0.1 cm^2 (based on gold oxide stripping in dilute perchloric acid). The Au beads were annealed in a natural gas-air flame, oxidized in 0.1 M $HClO_4$ at a current density of 0.3 A/cm^2, and dipped in dilute HCl to dissolve the copper-colored oxide layer. Cyclic voltammograms in 0.1 M $HClO_4$ were performed to ensure the cleanliness of the gold surface and to reduce any oxide layers remaining on the gold. Pt beads were cleaned by annealing in a natural gas−air flame followed by repeatedly cycling the potential through the oxide formation, oxide reduction, and hydrogen adsorption regions in 0.1 M $HClO_4$. Ag beads were flame-annealed and etched by briefly applying a potential sufficient to oxidize the silver in 0.1 M $HClO_4$ solution. All three types of electrodes were rinsed with water and ethanol and immersed in a dilute $HS(CH_2)_{15}COOH$ solution in ethanol (2 mg in 10 mL) for 48 h.

The base electrolyte for all experiments was room temperature (22 °C) 0.5 M NaF adjusted to pH 5 using trifluoroacetic acid. The SAM-coated Au and Pt electrodes were examined by CV in the base electrolyte between −0.5 and +0.5 V vs SCE. The positive potential limit for Ag electrodes was +0.2 V vs SCE to avoid Ag oxidation visible even on SAM-coated electrodes. If satisfactory behavior was observed (low potential-independent charging current), the electrodes were immersed for 5 min in an argon-saturated solution containing 15 mL of pH 7 phosphate buffer (5 mM), 0.15 g of KNO_3, 6 mg of Ru(4-AMP), and 0.15 g of EDC. In this solution, the Ru(4-AMP) rapidly couples to the pendant carboxylic acid groups on the SAM; the short immersion time is designed to keep the coverage well below saturation coverage. After rinsing with water, each electrode was examined by CV in the base electrolyte. A single well-shaped wave near 0 V vs SCE was taken as evidence of a well-formed SAM with the redox centers attached to the external surface. The electrodes were rinsed and reimmersed in the ethanol thiol solution for 48 h to further anneal the SAM.

Attempts were made to form SAMs of $HS(CH_2)_{15}COOH$ on mercury film electrodes formed by electrochemical deposition of mercury on silver bead electrodes. These experiments were generally unsuccessful because of the frequent formation of multilayers rather than monolayers, the presence of an apparent desorption peak of the thiol layer at an inconvenient potential (−0.6 V vs SCE), and the appearance of an ill-defined redox wave for the Ru complex after the coupling reaction. Consequently, results for mercury electrodes are not reported.

Experiments were performed at room temperature (22−23 °C) in an acid-cleaned three-compartment cell filled with the base electrolyte. Dissolved air was removed by argon bubbling. Kinetic measurements were performed by CV over a wide scan rate range (0.02−1000 V/s in a 1−2−5 sequence) using a Princeton Applied Research model 273 potentiostat, a PAR model 175 waveform generator, and a Tektronix TDS 430A digital oscilloscope for data acquisition. Alternating current impedance spectroscopy at frequencies of 10−100 kHz were used to obtain the uncompensated resistance as the limiting value of the in-phase impedance. For the bead electrodes, typical uncompensated resistances and response times were 30−50 Ω and 10−30 μs, respectively.

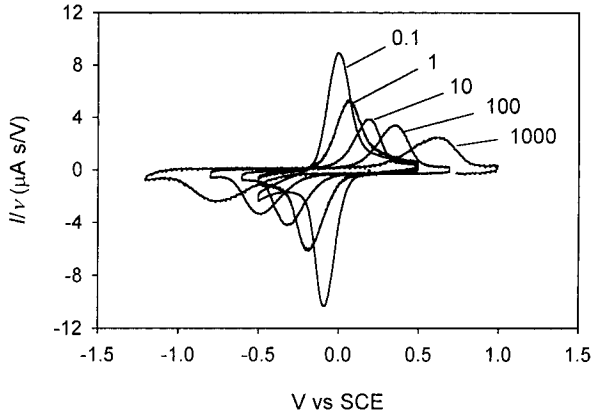

Figure 1. Scan-rate-normalized CVs of a gold bead coated with a $HS(CH_2)_{15}COOH$ SAM with attached $pyRu(NH_3)_5$ redox centers. Scan rates in V/s are shown. The electrolyte is 0.50 M NaF with the pH adjusted to 5.0. The initial potential is +0.20 V vs SCE, and the initial scan direction is negative. Anodic currents are positive.

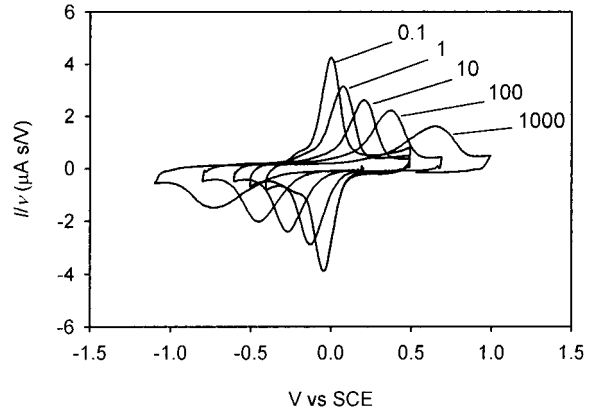

Figure 2. Scan-rate-normalized CVs of a platinum bead coated with a $HS(CH_2)_{15}COOH$ SAM with attached $pyRu(NH_3)_5$ redox centers. Other conditions are as in Figure 1.

Results

Rate constants at large overpotentials can be obtained by either chronoamperometry (potential step) or cyclic voltammetry (potential sweep). In these systems, CV is the preferred method because separation of charging and faradaic current is more easily accomplished. SAM-coated electrodes exhibit charging current curves that are nearly flat over a wide range of potentials. Extrapolation of the charging current underneath a faradaic peak can be performed with confidence if the charging current is visible on both sides of the faradaic peak. Figures 1, 2, and 3 are overlay plots of the scan-rate-normalized CVs for Au, Pt, and Ag, respectively. At all scan rates, the potential limits are extended so that the entire anodic or cathodic peak is visible in the CV. At most scan rates, the charging current is essentially linear with potential. At the smaller peak splittings observed at slower scan rates, the potential limits is kept within the range of potentials at which the SAM is stable in this electrolyte (−0.5 to +0.5 V vs SCE for Au). At larger peak splittings, it is necessary to extend the positive and negative potential limits beyond those normally imposed by water reduction and metal oxidation, both of which cause loss of the SAM, to fully define the anodic and cathodic faradaic current peaks. Fortunately, because these processes do not occur significantly during very

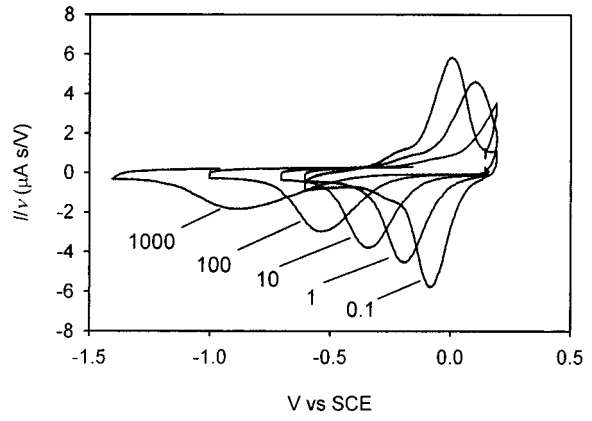

Figure 3. Scan-rate-normalized CVs of a silver bead coated with a $HS(CH_2)_{15}COOH$ SAM with attached $pyRu(NH_3)_5$ redox centers. The initial potential is +0.15 V vs SCE and the initial scan direction is negative. Other conditions are as in Figure 1.

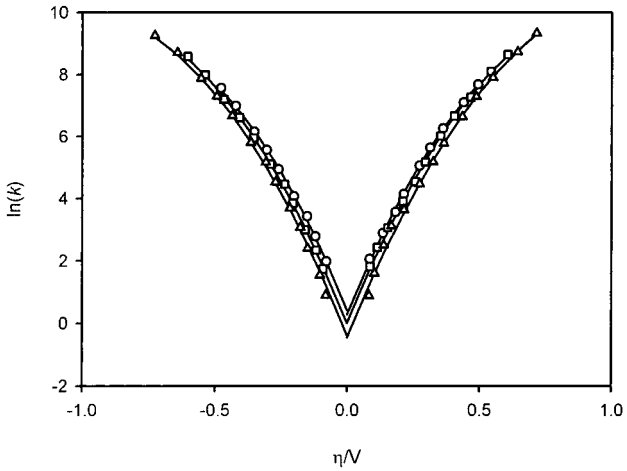

Figure 4. Tafel plots for a gold bead. The symbols are the data points, and the lines are the best-fit theoretical Tafel lines. Charge remaining 80% (circles); $k_{an}^0 = 1.3\ s^{-1}$, $k_{cat}^0 = 1.5\ s^{-1}$; $\lambda_{an} = 0.75$ eV, $\lambda_{cat} = 0.70$ eV. Charge remaining 50% (squares); $k_{an}^0 = 1.0\ s^{-1}$, $k_{cat}^0 = 1.0\ s^{-1}$; $\lambda_{an} = 0.85$ eV, $\lambda_{cat} = 0.80$ eV. Charge remaining 20% (triangles); $k_{an}^0 = 0.64\ s^{-1}$, $k_{cat}^0 = 0.68\ s^{-1}$; $\lambda_{an} = 0.90$ eV, $\lambda_{cat} = 0.85$ eV.

short excursions to the extreme potentials at scan rates of 100 V/s and up, faradaic currents can be obtained at overpotentials up to ±1 V on Au and Pt. Only the cathodic faradaic currents are analyzed on Ag due to the need to avoid potentials greater than +0.2 V vs SCE. Silver oxidation occurs at more positive potentials even at high scan rates. In all cases, CV data are acquired as a single scan at a given scan rate to avoid possible damage induced by multiple potential scans to extremes of potential. The success of this precaution is indicated by the constant coverage of redox centers over the duration of the data acquisition (see below).

Data analysis is done on a spreadsheet. The positive- or negative-going potential scan data are analyzed separately. A second-order charging current baseline is extrapolated from before the faradaic peak to after the faradaic peak and subtracted to isolate the faradaic current. The second-order extrapolation is needed to better match some curved charging currents seen at either slow scan rates or at large overpotentials. The peak potentials of the faradaic current are located. The formal potential $E^{\circ\prime}$ is obtained from the average of the peak positions at the slower scan rates. The redox centers are assumed to be thermodynamically homogeneous (same formal potential). This assumption is supported by the nearly ideal peak half-widths observed at the slowest scan rates (110−120 mV/s at 0.02 V/s; the ideal peak half-width is 91 mV). Potentials are converted to iR-corrected overpotentials

$$\eta(t) = E(t) - E^{\circ\prime} - i(t)R_u \qquad (5)$$

where $i(t)$ is the total current flowing at time t and R_u is the uncompensated resistance. Equation 5 assumes that the current density (and hence the overpotential) is uniform across the electrode surface. The faradaic current is integrated to yield the total faradaic charge Q_{tot} and the charge associated with the reactant state $Q(t)$ [Ru(III) for negative-going scans, Ru(II) for positive-going scans]:

$$Q_{tot} = \int i_f(t)\,dt \quad \text{(over the entire faradaic wave)} \qquad (6)$$

$$Q(t) = Q_{tot} - \int i_f(t)\,dt \quad \text{(from time 0 to time } t\text{)} \qquad (7)$$

Q_{tot} is proportional to the coverage of redox centers in the SAM. Ideally, it should be independent of the scan direction and scan rate and constant over the duration of the experiment. At a given scan rate, anodic and cathodic Q_{tot} values agree within 10%. CVs recorded at 0.1 V/s at the beginning and end of the experiment yield the same Q_{tot}. This observation confirms the stability of the Ru redox centers even after excursions to very negative or very positive potentials at high scan rates. Coverages calculated from Q_{tot} at slow scan rates correspond to 15−50% of the maximum coverage attainable (20 μcoul/cm^2 or 2×10^{-10} mol/cm^2) for this redox center.[22] The variation in coverage for each electrode preparation appears to be caused by small differences in the coupling reaction conditions and the annealing step. The coverage does not appear to be dependent on the metal. Maximum coverages are avoided in order to minimize possible lateral interactions between proximate redox centers. When the coverages are on the order of 15−30% of the maximum coverage, Q_{tot} is independent of the scan rate. At higher coverages, Q_{tot} decreased by as much as 50% going from 0.1 to 1000 V/s. This apparent loss of coverage is not understood. In these cases, the kinetic analysis is based on the Q_{tot} observed at the given scan rate.

At any overpotential more than 100 mV beyond $E^{\circ\prime}$, the rate constant is given by the ratio of the instantaneous faradaic current to the charge remaining:

$$k(t) = i_f(t)/Q(t) \qquad (8)$$

In principle, rate constant data can be obtained over a range of overpotentials of 0.2−0.4 V in a single voltammogram, the range at which faradaic currents are significant. The range is dictated by the scan rate, since higher scan rates shift the faradaic wave to larger overpotentials (Figures 1−3). In principle, a single faradaic peak could be fitted to the above equations to extract the standard rate constant and reorganization energy. Unfortunately, such an analysis is distorted by kinetic heterogeneity, which is the spread of rate constants for the ensemble of redox centers. In a linear scan experiment, the current at lower overpotentials (shorter time) is dominated by electron transfer to the kinetically faster redox centers, while the current at larger overpotentials (longer time) is controlled by electron transfer to the kinetically slower redox centers. Consequently, the faradaic peak is broader than expected for a given standard rate constant and reorganization energy. Analysis of a single faradaic peak using a single standard rate constant and reorganization energy leads to an anomalously low value for the reorganization

TABLE 1: Summary of Kinetic Parameters[f]

	k_{an}^0/s^{-1}			k_{cat}^0/s^{-1}			λ_{an}/eV			λ_{cat}/eV		
	80%	50%	20%	80%	50%	20%	80%	50%	20%	80%	50%	20%
Gold												
avg[a]	1.3	0.91	0.64	1.4	0.98	0.67	0.77	0.90	0.92	0.72	0.80	0.86
SD[a]	0.1	0.11	0.14	0.2	0.10	0.11	0.04	0.07	0.06	0.04	0.03	0.03
avg[b]		0.94			1.0			0.86			0.79	
SD[b]		0.29			0.4			0.09			0.07	
avg[c]		0.98						0.83				
SD[c]		0.32						0.09				
Platinum												
avg[d]	2.2	1.8	1.4	2.2	1.6	1.0	0.68	0.78	0.82	0.65	0.75	0.82
SD[d]	0.1	0.1	0.2	0.1	0.1	0.1	0.04	0.04	0.04	0.00	0.00	0.04
avg[b]		1.8			1.6			0.76			0.74	
SD[b]		0.4			0.5			0.07			0.08	
avg[c]		1.7						0.75				
SD[c]		0.4						0.07				
Silver												
avg[e]				0.74	0.60	0.41				0.71	0.75	0.80
SD[e]				0.07	0.08	0.10				0.06	0.04	0.04
avg[b]					0.58						0.75	
SD[b]					0.16						0.06	

[a] Average and standard deviation for six independent experiments. [b] Average and standard deviation for anodic or cathodic parameters. [c] Global average for each metal. [d] Average and standard deviation for two independent experiments. [e] Average and standard deviation for four independent experiments. [f] The column headers of 80%, 50%, and 20% refer to the amount of reactant remaining (Ru(II) for anodic parameters, Ru(III) for cathodic parameters).

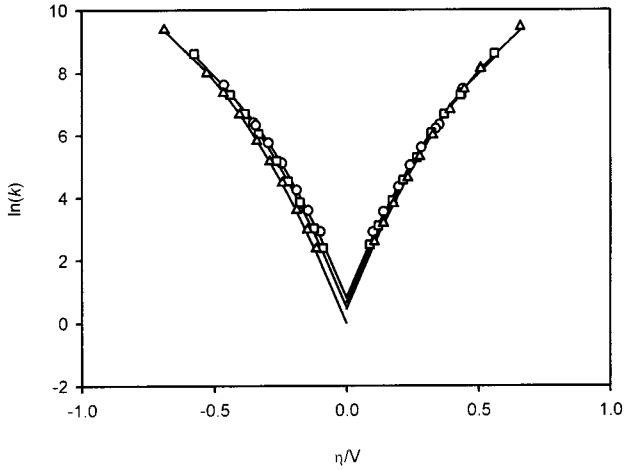

Figure 5. Tafel plots for a platinum bead. Charge remaining 80% (circles); $k_{an}^0 = 2.3\ s^{-1}$, $k_{cat}^0 = 2.2\ s^{-1}$; $\lambda_{an} = 0.65$ eV, $\lambda_{cat} = 0.65$ eV. Charge remaining 50% (squares); $k_{an}^0 = 1.9\ s^{-1}$, $k_{cat}^0 = 1.6\ s^{-1}$; $\lambda_{an} = 0.75$ eV, $\lambda_{cat} = 0.75$ eV. Charge remaining 20% (triangles); $k_{an}^0 = 1.6\ s^{-1}$, $k_{cat}^0 = 1.0\ s^{-1}$; $\lambda_{an} = 0.80$ eV, $\lambda_{cat} = 0.85$ eV.

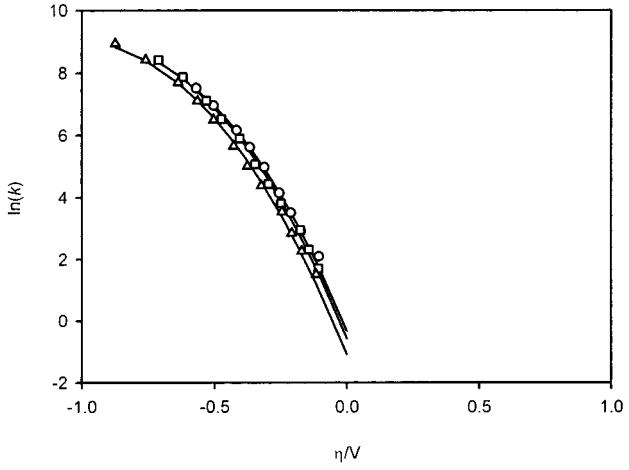

Figure 6. Tafel plots for a silver bead. Charge remaining 80% (circles); $k_{cat}^0 = 0.72\ s^{-1}$; $\lambda_{cat} = 0.70$ eV. Charge remaining 50% (squares); $k_{cat}^0 = 0.57\ s^{-1}$; $\lambda_{cat} = 0.75$ eV. Charge remaining 20% (triangles); $k_{cat}^0 = 0.34\ s^{-1}$; $\lambda_{cat} = 0.80$ eV.

energy.[23] In the analysis used by Murray and co-workers, the plot of peak potential vs scan rate is fitted to theoretical working curves over a wide range of scan rates. Simulation of linear scan voltammograms with kinetic heterogeneity indicates that the fit represents "average" values for k^0 and λ for the ensemble of redox centers.[23] This approach is valid only if iR drop is negligible for all parts of the CV. In the experiments reported here, iR drop is significant (>10 mV) at the highest scan rates.

Our approach to evaluating the behavior of a kinetically heterogeneous system assumes that the various populations of faster and slower redox centers can be defined by charge segments in the faradaic wave. In each linear voltage scan, rate constants are obtained at times corresponding to 80%, 50%, and 20% of the charge remaining ($Q(t)/Q_{tot}$) and paired with the corresponding iR-drop-corrected overpotentials. Each set of data (percent charge remaining, cathodic or anodic rate constants) is independently fitted to theoretical Tafel curves from eq 1 by least squares minimization. The theoretical Tafel curves are calculated for 25 °C; the differences caused by the discrepancy between the experimental temperature and 25 °C are negligible. To aid the fitting procedure, the theoretical Tafel curves are simulated using the following equations:[24]

$$\ln(k) = \ln(k^0) - \alpha(\eta)\eta/(0.02569) \quad (9)$$

$$\alpha(\eta) = 0.5 \pm a\eta \pm b\eta^3 \pm c\eta^5 \quad (10)$$

In eq 10, a, b, and c are parameters obtained by nonlinear regression fitting of eqs 9 and 10 to the theoretical Tafel curves; for example, $a = -0.2739$, $b = 0.01232$, and $c = 0.005753$ for $\lambda = 0.8$ eV. The "+" signs are used for anodic rate constants and the "−" signs for cathodic rate constants. For data extending to overpotentials greater than 0.5 V, the fit yields the standard rate constant k^0 (k at $\eta = 0$ V) and λ with an uncertainty of ±0.05 eV. The standard rate constant is also determined from the peak splitting, where ΔE_p was between 20 and 200 mV.[25] The working curve relating k^0 to peak splitting is relatively insensitive to λ under these conditions.[23,26]

Representative Tafel plots for Au, Pt, and Ag are shown in Figures 4, 5, and 6, respectively. Each plot contains the data points obtained from CVs at different scan rates and the best-fit theoretical Tafel line. The fits are very good; the root-mean-square deviation between the ln(k) data and the theoretical Tafel lines is typically less than 0.1.

The kinetic parameters for all measurements on all three types of electrodes are summarized in Table 1. For each type of electrode, several trends are evident. Kinetic heterogeneity is reflected in the decreasing k^0 values as the percent of reactant oxidation state decreases. There appears to be a corresponding increase in the reorganization energies, which may be the origin of the heterogeneity in the standard rate constant. Comparison of anodic vs cathodic parameters shows no statistically significant difference in k^0 or λ on platinum as well as on gold. We do not anticipate that silver would deviate from this pattern. Consequently, global average values for gold and platinum and the cathodic average values for silver are used in subsequent discussion.

Discussion

Experiments on each metal are repeated several times under conditions as identical as possible. Within experimental uncertainty, λ is 0.8 ± 0.1 eV, independent of the metal (Table 1). This observation is consistent with the idea that the redox centers are insulated by the relatively thick alkane layer from the physical and chemical properties associated with the different metals. It is therefore possible to compare standard rate constants between the metals without having to correct for variations in the reorganization energy.

This set of experiments and many previous experiments in our laboratory consistently yield a k^0 of 1.0 s^{-1} for gold with a SAM composed of $HS(CH_2)_{15}COOH$ + Ru(4-AMP). In accordance with predictions of Gosavi and Marcus,[2] k^0 for Pt is a factor of 1.7 higher than k^0 for Au and clearly not a factor of 7.5 based on the ratio of the density of states at the Fermi energy. Au and Ag both have only sp states near the Fermi energy. The smaller k^0 for Ag is in agreement with the electronic heat constants (which is proportional to density of states near the Fermi energy) of the two metals (0.65 for Ag, 0.73 for Au).[27]

The excellent agreement with theory is perhaps fortuitous for several reasons. First, the metals used in these experiments are polycrystalline, while the calculations of Gosavi and Marcus are for the (111) face of gold and platinum.[28] Second, not only do the metals have different electrochemical properties (potential of zero charge, for example) but the SAMs on each metal are certain to exhibit slight differences in average orientation and tilt. The degree to which these factors affect the electronic coupling are still unknown. Third, kinetic heterogeneity and the variation of kinetics for independent experiments make the average values somewhat uncertain, about ±30% for k^0 and about ±0.1 eV for λ. Nevertheless, the results obtained in these experiments clearly support the prediction that d band states in the metal contribute relatively little to the electronic coupling in long-range electron transfer.

Conclusions

We have performed kinetic measurements of one type of SAM [$(HSCH_2)_{15}COOH$ with attached Ru(4-AMP) redox centers] on three metals (Au, Pt, Ag) in one electrolyte at one temperature. Within experimental uncertainty, the reorganization energy of the Ru redox center is independent of the metal. The average standard rate constants for Au, Pt, and Ag are 1.0, 1.7, and 0.6 s^{-1}. The ratio of standard rate constants for Pt relative to Au is considerably smaller than the factor of 7.5 expected on the basis of the density of states near the Fermi energy in each metal. The agreement with theory supports the prediction that d band states of the metal couple weakly to the remote redox centers on the SAM.

Acknowledgment. This work was supported by the National Science Foundation grant CHE-9711779.

References and Notes

(1) Finklea, H. O. *Electroanal. Chem.* **1996**, *19*, 109−335.
(2) Gosavi, S.; Marcus, R. A. *J. Phys. Chem. B* **2000**, *104*, 2067−2072.
(3) Hsu, C.-P.; Marcus, R. A. *J. Chem. Phys.* **1997**, *106*, 584−598.
(4) Marcus, R. A. *J. Chem. Soc., Faraday Trans.* **1996**, *92*, 3905−3908.
(5) Smalley, J. F.; Feldberg, S. W.; Chidsey, C. E. D.; Linford, M. R.; Newton, M. R.; Liu, Y.-P. *J. Phys. Chem.* **1995**, *99*, 13141−13149.
(6) Finklea, H. O.; Hanshew, D. D. *J. Am. Chem. Soc.* **1993**, *114*, 3173−3181.
(7) Finklea, H. O.; Liu, L.; Ravenscroft, M. S.; Punturi, S. *J. Phys. Chem.* **1996**, *100*, 18852−18858.
(8) Dubois, L. H.; Nuzzo, R. G. *Annu. Rev. Phys. Chem.* **1992**, *43*, 437−463.
(9) Chidsey, C. E. D. *Science* **1991**, *251*, 919−922.
(10) Weber, K.; Hockett, L.; Creager, S. *J. Phys. Chem. B* **1997**, *101*, 8286−8291.
(11) Bowden, E. F. *Interface* **1997**, *6*, 40−44.
(12) El Kasmi, A.; Wallace, J. M.; Bowden, E. F.; Binet, S. M.; Linderman, R. J. *J. Am. Chem. Soc.* **1998**, *120*, 225−226.
(13) Song, S.; Clark, R. A.; Bowden, E. F.; Tarlov, M. J. *J. Phys. Chem.* **1993**, *97*, 6564−6572.
(14) Becka, A. M.; Miller, C. J. *J. Phys. Chem.* **1992**, *96*, 2657−2668.
(15) Miller, C.; Cuendet, P.; Gratzel, M. *J. Phys. Chem.* **1991**, *95*, 877−886.
(16) Miller, C.; Gratzel, M. *J. Phys. Chem.* **1991**, *95*, 5225−5233.
(17) Gadzuk, J. W.; Plummer, E. W. *Rev. Modern Phys.* **1973**, *45*, 487−547.
(18) Capon, A.; Parsons, R. *J. Electroanal. Chem.* **1973**, *46*, 215−222.
(19) Li, T. T. T.; Weaver, M. J. *J. Am. Chem. Soc.* **1984**, *106*, 6107−6108.
(20) Li, T. T. T.; Liu, H. Y.; Weaver, M. J. *J. Am. Chem. Soc.* **1984**, *106*, 1233−1239.
(21) Iwasita, T.; Schmickler, W.; Schultze, J. W. *Ber. Bunsen-Ges.Phys. Chem.* **1985**, *89*, 138−142.
(22) Finklea, H. O.; Hanshew, D. D. *J. Electroanal. Chem.* **1993**, *347*, 327−340.
(23) Tender, L.; Carter, M. T.; Murray, R. W. *Anal. Chem.* **1994**, *66*, 3173−3181.
(24) Finklea, H. O. *J. Electroanal. Chem.* **2001**, *495*, 79−86.
(25) Laviron, E. *J. Electroanal. Chem.* **1979**, *101*, 19−28.
(26) Rowe, G. K.; Carter, M. T.; Richardson, J. N.; Murray, R. W. *Langmuir* **1995**, *11*, 1797−1806.
(27) Kittel, C. *Introduction to Solid State Physics*; John Wiley & Sons: New York, 1971; pp 252−255.
(28) Marcus, R. A. Personal communication.